Magnetic microrobot control using an adaptive fuzzy sliding-mode method

Alireza Mousavi, Hesam Khaksar, Awais Ahmed, Hongsoo Choi, *Senior Member*, *IEEE*, and Ali Kafash Hoshiar, *Member*, *IEEE*

***Abstract*—The magnetic medical microrobots are influenced by diverse factors such as the medium, the geometry of the microrobot, and the imaging procedure. It is worth noting that the size limitations make it difficult or even impossible to obtain reliable physical properties of the system. In this research, to achieve a precise microrobot control using minimum knowledge about the system, an Adaptive Fuzzy Sliding-Mode Control (AFSMC) scheme is designed for the motion control problem of the magnetically actuated microrobots in presence of input saturation constraint. The AFSMC input consists of a fuzzy system designed to approximate an unknown nonlinear dynamical system and a robust term considered for mismatch compensation. According to the designed adaptation laws, the asymptotic stability is proved based on the Lyapunov theorem and Barbalat's lemma. In order to evaluate the effectiveness of the proposed method, a comparative simulation study is conducted.**

***Index Terms*— Medical Robots and Systems, Micro/Nano Robots, Motion Control.**

I. Introduction

Over the past decade, the magnetically actuated microrobots have shown high potential in medical applications. These applications include a wide range of therapeutic processes including cancer treatment [1], [2], vascular interventions [3], [4], tumor-targeting therapy [5], targeted drug delivery [3], [6], [7], hyperthermia therapy [8], and microsurgery. The main reasons for the use of the microrobots are their suitable dimensions and soft deformable structure [3]. However, the major challenge in the microrobot control is the existence of the environmental uncertainties (e.g. the medium). Moreover, the effects of viscous forces dominating inertia forces should be considered.

Previously, different methods have been proposed for the manipulation of the microrobots. In [9], a tele-microrobot system was used to manipulate microscopic objects. Moreover, in [10], medical magnetic resonance imaging (MRI) gradient coils were employed to generate a magnetic field and drive a microrobot. Due to the safety of magnetic actuation systems, dexterity in the field generation, and precise field control, they have emerged as the preferred method of actuation [11]. The earlier electromagnetic actuation system consists of the Helmholtz and Maxwell coils. The Helmholtz coils are used to produce uniform magnetic flux density, while the Maxwell coils are employed for generating linear gradient fields [12]. Dedicated multi-coil magnetic actuation systems for microrobots have been developed [13]. Fig. 1 illustrates the schematic of a magnetic control system.

The magnetic manipulation process is influenced by several factors including the characteristics of the medium, the geometry of the microrobot, and the imaging procedure. The manipulation can be done in different mediums. However, considering the medical applications, the modeling of this process should be performed in a liquid medium similar to the biological environments leading to an increase in the uncertainty and complexity [14], [15]. Depending on the swimming mechanism, the geometry of the microrobots in previous studies has often been selected as helical [16], [17], cylindrical [18], hexahedral or spherical [19] shapes. Moreover, in the manipulation control, image-based sensors including fluoroscopy [20], optical cameras [21], and magnetic resonance images [22] have been used to detect the exact position of the microrobot. Depending on the various parameters affecting the problem, such as the medium and the geometry of the microrobot, different control methods can be employed.

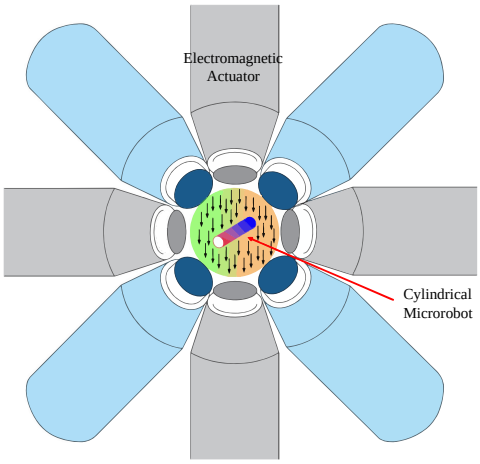

Fig.1. Schematic of the microrobot control system

This work is supported by University of Essex, Robotics and Embedded System research group. (Corresponding author: Ali Kafash Hoshiar)

Alireza Mousavi, Hesam Khaksar, and Ali Kafash Hoshiar are with the School of Computer Science and Electronic Engineering, University of Essex, Colchester, CO4 3SQ, UK (email: a.kafashhoshiar@essex.ac.uk).

Alireza Mousavi is also with Iran University of Science and Technology, Tehran, 1684613114, Iran.

Awais Ahmed and Hongsoo Choi are with the Department of Robotics Engineering and the DGIST-ETH Microrobot Research Center, Daegu Gyeongbuk Institute of Science and Technology, Daegu 42988, South Korea.

Previously, several control methods have been proposed for the motion control of the microrobots. According to [23], the PID control method has unsatisfactory tracking performance in the position control problem of the microrobot. Moreover, adaptive PID control [23], adaptive backstepping control [24], optimal control [25], [26], recursive least square control [21], and H-infinity control [27] have been proposed to improve the tracking performance. However, their performances are inadequate for medical applications. It is worth noting that, they require model information [24], [25], [27] and most of them have been developed for 2-DOF position control of the microrobot [21], [23], [24], [26].

Recently, a robust control law which is called "time-delay control" has been presented for the 3-DOF motion control of the microrobot based on the concept of the time-delay estimation [14]. In this method, there is no need to employ precise model information. Furthermore, the time-delay control shows a faster response, smaller overshoot, and reduced steady-state error as compared with the abovementioned control schemes. Since the time-delay control method can cause the windup phenomenon, a time-delay estimation-based control law has been developed in [28] which includes an anti-windup scheme as well as a switching term with an integral sliding surface to avoid the windup, and a forgetting factor to attenuate the accumulating effect of the measurement error.

To implement the time-delay control method with an anti-windup scheme, the nominal value of the mass matrix should be employed which is hard or impossible to obtain. Furthermore, in this method, some constant matrices should be selected based on the Lyapunov stability theorem. Hence, users may face some difficulties to tune the controller. It is worth noting that, this method may cause high-frequency velocity fluctuations and steady-state position error.

In this research, to improve the position tracking performance without using the nominal value of the mass matrix, an adaptive fuzzy sliding-mode control (AFSMC) scheme is proposed. The AFSMC input consists of a fuzzy system and a robust term. The fuzzy system is employed to approximate an unknown nonlinear dynamical system and the robust term is designed to compensate for the approximation error. Moreover, the adaptation laws are obtained based on the second Lyapunov theorem. It is worth noting that, in this method, the effect of input saturation is considered as an uncertainty term.

The rest of the manuscript is organized as follows: In Section II, the dynamic equations of the system are presented. In Section III, the proposed AFSMC scheme is expressed and the asymptotic stability is proved based on the Lyapunov theorem and Barbalat's lemma. In Section IV, the effectiveness of the proposed scheme is evaluated through numerical simulations and laboratory test results. Finally, conclusions are given in Section V.

II. Problem Definition

In the magnetic manipulation, the magnetic force $\mathbf{F}_m$, the drag force $\mathbf{F}_d$, the lift force $\mathbf{F}_l$, the buoyant force $\mathbf{F}_b$, and the weight

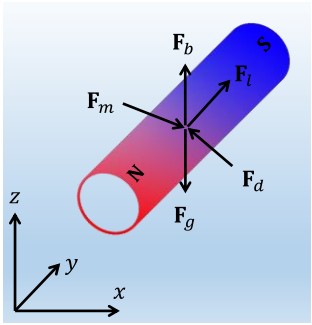

Fig.2. The free-body diagram of the magnetic cylindrical microrobot

$\mathbf{F}_g$ affect the motion of the magnetic cylindrical microrobot in a viscous fluid environment (see Fig. 2). In this problem, since it is difficult or even impossible to obtain the physical properties of the system (such as mass, volume, and viscosity), terms $\mathbf{F}_d$, $\mathbf{F}_l$, $\mathbf{F}_b$, and $\mathbf{F}_g$ are assumed to be unknown. Furthermore, the control input $\mathbf{F}_m$ is generated as

$$\mathbf{F}_m = (\mathbf{M} \cdot \nabla)\mathbf{B} \tag{1}$$

where $\mathbf{B} \in \mathbb{R}^{3\times1}$ denotes the magnetic field vector generated by electromagnets, ∇ is the gradient operator, and $\mathbf{M} \in \mathbb{R}^{3\times1}$ stands for the magnetic momentum [28]. Since the direction of the magnetic field does not change quickly, it is assumed that the microrobot and the magnetic field vector $\mathbf{B}$ are in the same direction. Therefore, by defining the direction vector of $\mathbf{B}$ in the form of

$$\hat{\mathbf{u}}_\mathbf{B} = \frac{\mathbf{B}}{\|\mathbf{B}\|} = \frac{\mathbf{M}}{\|\mathbf{M}\|}, \tag{2}$$

the magnetic force $\mathbf{F}_m$ is represented as

$$\mathbf{F}_m = \|\mathbf{M}\| \begin{bmatrix} \partial\mathbf{B}/\partial x \\ \partial\mathbf{B}/\partial y \\ \partial\mathbf{B}/\partial z \end{bmatrix} \hat{\mathbf{u}}_\mathbf{B} = \begin{bmatrix} \partial\mathbf{B}/\partial x \\ \partial\mathbf{B}/\partial y \\ \partial\mathbf{B}/\partial z \end{bmatrix} \mathbf{M}. \tag{3}$$

In this problem, it is assumed that the coils are ideal. Moreover, by considering a linear response of the magnetic cores, the magnetic field is described by the linear superposition of the individual fields of the electromagnetic coils [29]. The magnetic field of each coil is proportional to its corresponding current. Hence, by introducing the set of currents in the coils $\mathbf{I}$ and the coefficient matrix $\mathbf{K}$, we have

$$\mathbf{F}_m = \mathbf{K}(\mathbf{X}, \mathbf{M})\mathbf{I} \tag{4}$$

where $\mathbf{X} = [x, y, z]^\mathrm{T}$ is the position vector of the microrobot. In order to find the required currents of the coils using (4), the coefficient matrix $\mathbf{K}$ is modeled and calibrated to map the magnetic field $\mathbf{B}$ and the gradient field at any position within the robot workspace [29].

Since the assumption (2) is not perfectly valid, the uncertainty force $\mathbf{F}_\Delta$ should be considered in the structure of the dynamic equation. It is worth noting that, $\mathbf{F}_\Delta$ represents several forces, such as the inertial force due to the added-mass effect, the contact force at the fluid container surface, the van

der Waals force, and the electrostatic force [28]. The aforementioned forces have not been modeled due to their complexity.

Due to the limitations of the magnetic actuator, the control input saturation should be considered in the dynamic model of the system. Hence, by introducing m as the mass of the microrobot, the three degree-of-freedom equation of motion is presented as

$$\ddot{\mathbf{X}} = \frac{1}{m}\mathrm{sat}(\mathbf{F}_m) + \frac{1}{m}\left(\mathbf{F}_d + \mathbf{F}_l + \mathbf{F}_g + \mathbf{F}_b + \mathbf{F}_\Delta\right) \tag{5}$$

where

$$\mathrm{sat}(\mathbf{F}_m) = \begin{cases} \mathbf{F}_{m,\max}, & \mathbf{F}_m \geq \mathbf{F}_{m,\max} \\ \mathbf{F}_m, & \mathbf{F}_{m,\min} \leq \mathbf{F}_m \leq \mathbf{F}_{m,\max} \\ \mathbf{F}_{m,\min}, & \mathbf{F}_m \leq \mathbf{F}_{m,\min} \end{cases} \tag{6}$$

and $\mathbf{F}_{m,\min}$ and $\mathbf{F}_{m,\max}$ respectively denote the lower and the upper saturation limits. In this problem, the effect of input saturation is considered as an uncertainty term in the form of

$$\mathbf{d}' = \frac{1}{m}[\mathrm{sat}(\mathbf{F}_m) - \mathbf{F}_m]. \tag{7}$$

Thus, the lumped uncertainty term is defined as

$$\mathbf{d} = \frac{1}{m}\left(\mathbf{F}_d + \mathbf{F}_l + \mathbf{F}_g + \mathbf{F}_b + \mathbf{F}_\Delta\right) + \mathbf{d}' \tag{8}$$

and the dynamic equation of the system is represented in the form of

$$\ddot{\mathbf{X}} = \frac{1}{m}\mathbf{F}_m + \mathbf{d}. \tag{9}$$

Hence, by defining the desired position vector $\mathbf{X}_d = [x_d, y_d, z_d]^{\mathrm{T}}$, the control objective here is to achieve $\lim_{t\to\infty} \mathbf{X} = \mathbf{X}_d$.

III. Design of the Adaptive Fuzzy Sliding-mode Control Structure

In order to design the adaptive control structure, by introducing the error vector in the form of

$$\tilde{\mathbf{X}} = \mathbf{X}_d - \mathbf{X}, \tag{10}$$

the sliding vector is defined as

$$\mathbf{s} = \dot{\tilde{\mathbf{X}}} + \boldsymbol{\lambda}\tilde{\mathbf{X}} \tag{11}$$

where $\boldsymbol{\lambda}$ is a diagonal positive definite matrix. According to (11), the time derivative of the sliding vector $\mathbf{s}$ is obtained as

$$\dot{\mathbf{s}} = \ddot{\mathbf{X}}_d - \mathbf{d} + \boldsymbol{\lambda}\left(\dot{\mathbf{X}}_d - \dot{\mathbf{X}}\right) - \frac{1}{m}\mathbf{F}_m. \tag{12}$$

In continuation, (12) can be written in the form of

$$m\dot{\mathbf{s}} = \boldsymbol{\beta}^* - \mathbf{F}_m \tag{13}$$

where

$$\boldsymbol{\beta}^* = [\beta_1^*, \beta_2^*, \beta_3^*]^{\mathrm{T}} = m\left(\ddot{\mathbf{X}}_d - \mathbf{d} + \boldsymbol{\lambda}\left(\dot{\mathbf{X}}_d - \dot{\mathbf{X}}\right)\right). \tag{14}$$

Since the value of $\boldsymbol{\beta}^*$ is unknown, 3 TSK fuzzy systems are employed to approximate $\beta_i^*, i = 1,2,3$. For the i-th fuzzy system, n_r IF-THEN rules are defined as below.

$$\text{If } s_i = A_i^r, \text{ then } \beta_i^{fuz} = b_i^r.$$

Here, $r = 1, \dots, n_r$, b_i^r is the output corresponding to the r-th rule of the i-th fuzzy system, and A_i^r is a fuzzy set. For $r = 2, \dots, n_r - 1$, A_i^r is characterized by Gaussian membership function

$$\mu_{A_i^r}(s_i) = \exp\left[-\frac{(s_i - c_i^r)^2}{2{\sigma_i^r}^2}\right] \tag{15}$$

with shape parameters c_i^r and σ_i^r. Moreover, for $r = 1$ and $r = n_r$, the membership function $\mu_{A_i^r}(s_i)$ is defined as

$$\mu_{A_i^r}(s_i) = \frac{1}{1 + \exp\left[-\frac{(s_i - c_i^r)}{\sigma_i^r}\right]}. \tag{16}$$

In this research, the singleton fuzzifier, the product inference, and the center average defuzzifier are employed. Hence, we have:

$$\beta_i^{fuz} = \frac{\sum_{r=1}^{n_r} b_i^r \mu_{A_i^r}(s_i)}{\sum_{r=1}^{n_r} \mu_{A_i^r}(s_i)}. \tag{17}$$

By defining w_i^r $(r = 1, \dots, n_r)$ as

$$w_i^r = \frac{\mu_{A_i^r}(s_i)}{\sum_{r=1}^{n_r} \mu_{A_i^r}(s_i)}, \tag{18}$$

The output of the i-th fuzzy system is generated as

$$\beta_i^{fuz} = \mathbf{b}_i^{\mathrm{T}}\mathbf{w}_i \tag{19}$$

where $\mathbf{b}_i = \left[b_i^1, \dots, b_i^{n_r}\right]^{\mathrm{T}}$ and $\mathbf{w}_i = \left[w_i^1, \dots, w_i^{n_r}\right]^{\mathrm{T}}$. Considering

$$\mathbf{b}_i^* \triangleq \arg\min_{\mathbf{b}_i}\left\{\left|\mathbf{b}_i^{\mathrm{T}}\mathbf{w}_i - \beta_i^*\right|\right\} \tag{20}$$

the minimum approximation error ψ_i is introduced as

$$\psi_i = \beta_i^* - \beta_i^{fuz}(s_i, \mathbf{b}_i^*) = \beta_i^* - \mathbf{b}_i^{*\mathrm{T}}\mathbf{w}_i \tag{21}$$

which is assumed to be bounded as $|\psi_i| \leq \Psi_i$ due to the general approximation of the fuzzy systems [30].

In this paper, the control input $\mathbf{F}_m = \left[F_{m_1}, F_{m_2}, F_{m_3}\right]^{\mathrm{T}}$ is generated according to

$$F_{m_i} = \hat{\beta}_i^{fuz} + u_i^{rb} \tag{22}$$

Where the fuzzy term $\hat{\beta}_i^{fuz}$ and the robust term u_i^{rb} are proposed as below.

$$\hat{\beta}_i^{fuz} = \hat{\mathbf{b}}_i^{\mathrm{T}}\mathbf{w}_i \tag{23}$$

$$u_i^{rb} = \widehat{\Psi}_i \mathrm{sgn}(s_i) \tag{24}$$

Here, $\hat{\mathbf{b}}_i$ and $\widehat{\Psi}_i$ respectively denote the approximated values of $\mathbf{b}_i^*$ and Ψ_i which are computed by the following adaptation laws.

$$\dot{\hat{\mathbf{b}}}_i = \alpha_{1_i} s_i \mathbf{w}_i \tag{25}$$

$$\dot{\widehat{\Psi}}_i = \alpha_{2_i}|s_i| \tag{26}$$

Furthermore, arbitrary positive parameters α_{1_i} and α_{2_i} ($i = 1,2,3$) are the learning rates of the adaptive control scheme.

Theorem. *Asymptotic stability of the dynamic system (9) is achieved by the control input (22) and adaptation laws (25) and (26).*

Proof. Based on approximation errors $\tilde{\mathbf{b}}_i = \mathbf{b}_i^* - \hat{\mathbf{b}}_i$ and $\widetilde{\Psi}_i = \Psi_i - \widehat{\Psi}_i$ ($i = 1,2,3$), the positive definite function V is defined as below.

$$V = \frac{1}{2} m \mathbf{s}^{\mathrm{T}} \mathbf{s} + \sum_{i=1}^{3} \frac{1}{2\alpha_{1_i}} \tilde{\mathbf{b}}_i^{\mathrm{T}} \tilde{\mathbf{b}}_i + \sum_{i=1}^{3} \frac{1}{2\alpha_{2_i}} \widetilde{\Psi}_i^2 \tag{27}$$

In continuation, the time derivative of V is obtained as

$$\dot{V} = \sum_{i=1}^{3} s_i \left(\beta_i^* - F_{m_i}\right) + \sum_{i=1}^{3} \frac{1}{\alpha_{1_i}} \tilde{\mathbf{b}}_i^{\mathrm{T}} \dot{\tilde{\mathbf{b}}}_i + \sum_{i=1}^{3} \frac{1}{\alpha_{2_i}} \widetilde{\Psi}_i \dot{\widetilde{\Psi}}_i. \tag{28}$$

According to $\dot{\hat{\mathbf{b}}}_i = -\dot{\tilde{\mathbf{b}}}_i$, $\dot{\widehat{\Psi}}_i = -\dot{\widetilde{\Psi}}_i$, and (22) to (26), we have:

$$\begin{aligned} \dot{V} &= \sum_{i=1}^{3} s_i \left(\beta_i^* - \hat{\beta}_i^{fuz} - \widehat{\Psi}_i \mathrm{sgn}(s_i)\right) - \sum_{i=1}^{3} s_i \tilde{\mathbf{b}}_i^{\mathrm{T}} \mathbf{w}_i - \sum_{i=1}^{3} \widetilde{\Psi}_i |s_i| \\ &= \sum_{i=1}^{3} s_i \left(\tilde{\mathbf{b}}_i^{\mathrm{T}} \mathbf{w}_i + \psi_i - \widehat{\Psi}_i \mathrm{sgn}(s_i)\right) - \sum_{i=1}^{3} s_i \tilde{\mathbf{b}}_i^{\mathrm{T}} \mathbf{w}_i - \sum_{i=1}^{3} \widetilde{\Psi}_i |s_i| \\ &= \sum_{i=1}^{3} s_i \psi_i - \sum_{i=1}^{3} \widehat{\Psi}_i |s_i| - \sum_{i=1}^{3} \left(\Psi_i - \widehat{\Psi}_i\right) |s_i| \\ &= \sum_{i=1}^{3} s_i \psi_i - \sum_{i=1}^{3} \Psi_i |s_i|. \end{aligned} \tag{29}$$

Moreover, using $s_i \psi_i \le |s_i||\psi_i|$, it is outlined that

$$\begin{aligned} \dot{V} &\le \sum_{i=1}^{3} |s_i||\psi_i| - \sum_{i=1}^{3} \Psi_i |s_i| \\ &= -\sum_{i=1}^{3} |s_i| (-|\psi_i| + \Psi_i) \le 0. \end{aligned} \tag{30}$$

Therefore, according to (30), s_i, $\tilde{\mathbf{b}}_i$, and $\widetilde{\Psi}_i$ remain bounded. Based on (12) and due to the boundedness of $\dot{\mathbf{s}}$, the sliding vector $\mathbf{s}$ is uniformly continuous for $t \ge 0$. In the following, the function Γ is defined as

$$\Gamma = \sum_{i=1}^{3} |s_i| (-|\psi_i| + \Psi_i) \le -\dot{V}. \tag{31}$$

By integrating Γ with respect to time, the following inequality is obtained.

$$\int_0^t \Gamma(\tau) d\tau \le V\left(\mathbf{s}(0), \tilde{\mathbf{b}}, \widetilde{\mathbf{\Psi}}\right) - V\left(\mathbf{s}(t), \tilde{\mathbf{b}}, \widetilde{\mathbf{\Psi}}\right) \tag{32}$$

Since $V\left(\mathbf{s}(0), \tilde{\mathbf{b}}, \widetilde{\mathbf{\Psi}}\right)$ is bounded and $V\left(\mathbf{s}(t), \tilde{\mathbf{b}}, \widetilde{\mathbf{\Psi}}\right)$ is non-increasing and bounded, $\lim_{t\to\infty} \int_0^t \Gamma(\tau) d\tau$ remains bounded. Furthermore, since Γ is continuous in bounded variables s_i ($i = 1,2,3$), Γ is uniformly continuous in t on $(0, +\infty)$. As a result, according to Barbalat's lemma [31], $\lim_{t\to\infty} \Gamma(t) = 0$, i.e., $\lim_{t\to\infty} \mathbf{s}(t) = 0$.

To reduce the chattering caused by robust control terms $u_i^{rb} = \widehat{\Psi}_i \mathrm{sgn}(s_i)$, the sign function $\mathrm{sgn}(s_i)$ can be replaced by saturation function $\mathrm{sat}(s_i)$. Accordingly, due to the asymptotic stability of the closed-loop system, variables s_i are driven into the saturation boundary layer.

IV. Simulation Results

In this section, the performance of the proposed control method is evaluated through numerical simulations. The specification of the microrobot submerged in the silicon oil of 1000-cSt viscosity is reported in [28] and $\mathbf{X}_d = [3, 2, 1]^{\mathrm{T}}$ (mm). The initial conditions of the controller are determined as $\hat{\mathbf{b}}_i(0) = [-0.1, -0.05, 0, 0.05, 0.1]^{\mathrm{T}}$ and $\widehat{\Psi}_i(0) = 0.1$. Furthermore, $\boldsymbol{\lambda} = \mathrm{diag}(100, 100, 30)$, $n_r = 5$, $\left[c_i^1, \dots, c_i^{n_r}\right] = [-0.3, -0.15, 0, 0.15, 0.3]$, $\left[\sigma_i^1, \dots, \sigma_i^{n_r}\right] = [-0.05, 0.05, 0.05, 0.05, 0.05]$, $\alpha_{1_i} = 0.1$, and $\alpha_{2_i} = 0.2$ are considered as the parameter values of the AFSMC. It should be noted that the learning rates of the AFSMC are fixed based on a trial-and-error selection procedure and the input space partitioning for the fuzzy model is arbitrarily chosen by the user based on prior knowledge about the satisfactory ranges of the tracking errors.

In order to conduct a comparative analysis, the performance of the AFSMC and the time-delay control method with an anti-windup scheme (presented by Kim et al. [28]) are compared. Using Kim's method, the simulation model is validated with experimental results reported in [28] (see Fig. 3). Since the dynamics of the magnetic actuator have not been considered in the simulation model, the rate of convergence in the reported experimental test has been rather low. Moreover, in the simulations corresponding to the Kim's method, it is assumed that the velocity of the microrobot is measured directly. To implement Kim's method, the nominal value of mass matrix $\bar{\mathbf{m}}$ should be employed. As it is shown in Fig. 3, the tracking performance of the Kim's method is affected by the choice of the nominal mass matrix. Furthermore, Kim's method causes high-frequency velocity fluctuations and steady-state position error.

As it is illustrated in Fig. 4, for $\bar{\mathbf{m}} = \mathrm{diag}(15 \times 10^{-6}, 14 \times 10^{-6}, 17 \times 10^{-6})$, the AFSMC method provides improved tracking performance versus Kim's method. In other words, the AFSMC enhances the convergence rate and the tracking precision. In practice, it is not possible to make direct measurements of the velocity. Therefore, an auxiliary algorithm is needed to estimate the velocity of the microrobot. In order to implement the adaptive fuzzy sliding-mode controller, Levant's exact differentiator [32] is employed for the velocity estimation. The effect of using Levant's differentiator as the velocity estimator on the tracking performance of the AFSMC method is shown in Fig. 4.

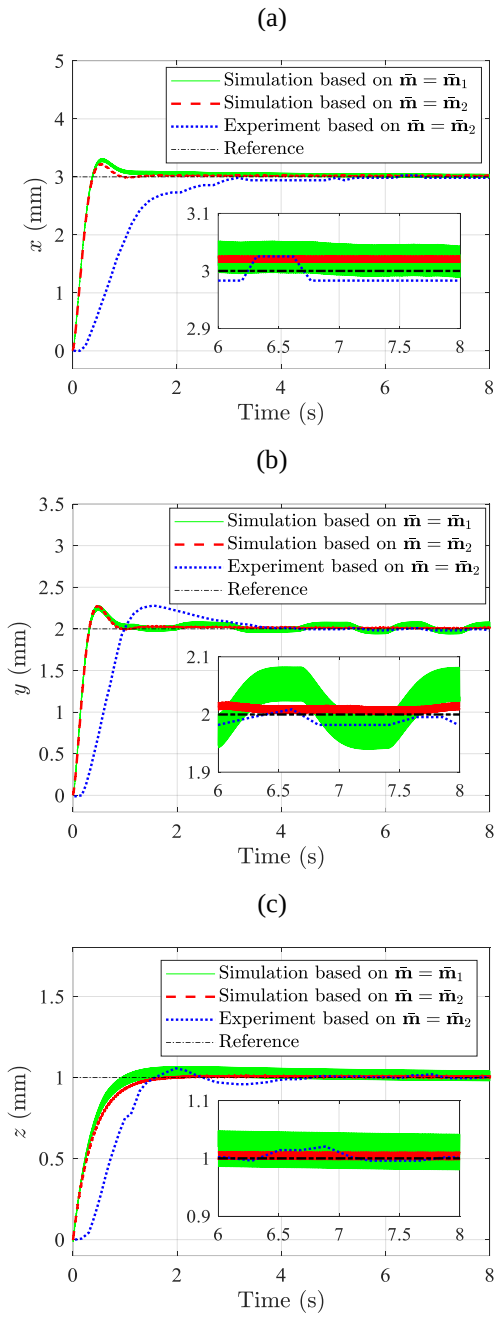

Fig.3. Tracking performance of the control method presented by Kim et al. for different values of $\bar{\mathbf{m}}$ ($\bar{\mathbf{m}}_1 = \mathrm{diag}(4\times10^{-6}, 4\times10^{-6}, 4\times10^{-6})$ and $\bar{\mathbf{m}}_2 = \mathrm{diag}(15\times10^{-6}, 14\times10^{-6}, 17\times10^{-6})$)

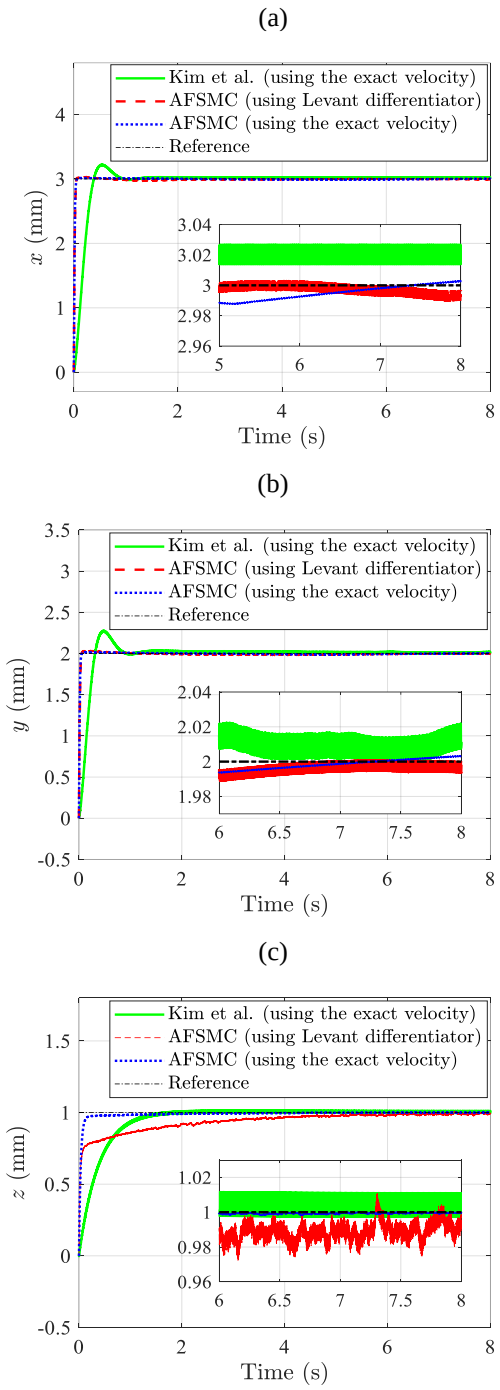

Fig.4. Tracking performance comparison of the control method presented by Kim et al. and the AFSMC method

Comparative analysis reveals that the adaptive fuzzy sliding-mode controller with the velocity estimator has an acceptable performance. However, the sign functions in the velocity estimation algorithm cause very low amplitude high-frequency fluctuations in the vicinity of the setpoint.

V. Conclusion

In this paper, to improve the position tracking performance of the electromagnetic actuated microrobots in the presence of input saturation, an adaptive fuzzy sliding-mode control (AFSMC) method was proposed. Contrary to the time-delay control method with the anti-windup scheme which is known as one of the most effective control methods in this application, there is no need to employ the nominal value of the mass matrix in the structure of the AFSMC. Furthermore, the tuning procedure of the adaptive controller will become rather simple. According to the simulation results, the AFSMC method improves the convergence rate and the tracking precision versus the time-delay control method with the anti-windup scheme. Moreover, in the AFSMC, the high frequency fluctuations in the vicinity of the setpoint are improved.

REFERENCES

[1] J. Han *et al.*, "Hybrid-Actuating Macrophage-Based Microrobots for Active Cancer Therapy," *Sci. Rep.*, vol. 6, no. 28717, 2016.

[2] V. Du Nguyen, V. H. Le, S. Zheng, J. Han, and J.-O. Park, "Preparation of tumor targeting cell-based microrobots carrying NIR light sensitive therapeutics manipulated by electromagnetic actuating system and Chemotaxis," *J. Micro-Bio Robot.*, vol. 14, no. 3–4, pp. 69–77, 2018.

[3] S. Jeon *et al.*, "A Magnetically Controlled Soft Microrobot Steering a Guidewire in a Three-Dimensional Phantom Vascular Network," *Soft Robot.*, vol. 6, no. 1, 2019.

[4] P. Lloyd, A. K. Hoshiar, T. da Veiga, and A. Attanasio, "A Learnt Approach for the Design of Magnetically Actuated Shape Forming Soft Tentacle Robots," *IEEE Robot. Autom. Lett.*, vol. 5, no. 3, pp. 3937–3944, 2020.

[5] D. Li *et al.*, "A hybrid actuated microrobot using an electromagnetic field and flagellated bacteria for tumor-targeting therapy: Hybrid Actuated Microrobot using EMA and Bacteria," *Biotechnol. Bioeng.*, vol. 112, no. 8, pp. 1623–1631, 2015.

[6] S. Lee *et al.*, "A Needle-Type Microrobot for Targeted Drug Delivery by Affixing to a Microtissue," *Adv. Healthc. Mater.*, vol. 9, no. 7, 2020.

[7] K. Abolfathi, M. R. H. Yazdi, and A. K. Hoshiar, "Studies of Different Swarm Modes for the MNPs Under the Rotating Magnetic Field," *IEEE Trans. Nanotechnol.*, vol. 19, pp. 849–855, 2020.

[8] J. Park, C. Jin, S. Lee, J.-Y. Kim, and H. Choi, "Magnetically actuated degradable microrobots for actively controlled drug release and hyperthermia therapy," *Adv. Healthc. Mater.*, vol. 8, no. 16, 2019.

[9] I. W. Hunter, S. Lafontaine, P. M. F. Nielsen, P. J. Hunter, and J. M. Hollerbach, "Manipulation and dynamic mechanical testing of microscopic objects using a tele-micro-robot system," *IEEE Control Syst. Mag.*, vol. 10, no. 2, pp. 3–9, 1990.

[10] S. Tamaz, R. Gourdeau, A. Chanu, J.-B. Mathieu, and S. Martel, "Real-Time MRI-Based Control of a Ferromagnetic Core for Endovascular Navigation," *IEEE Trans. Biomed. Eng.*, vol. 55, no. 7, pp. 1854–1863, 2008.

[11] T. Xu, J. Yu, X. Yan, H. Choi, and L. Zhang, "Magnetic actuation based motion control for microrobots: An overview," *Micromachines*, vol. 6, no. 9, pp. 1346–1364, 2015.

[12] C. Yu *et al.*, "Novel electromagnetic actuation (EMA) method for 3-dimensional locomotion of intravascular microrobot," *Sensors Actuators A Phys.*, vol. 161, no. 1–2, pp. 297–304, 2010.

[13] J. Hwang, J. Kim, and H. Choi, "A review of magnetic actuation systems and magnetically actuated guidewire- and catheter-based microrobots for vascular interventions," *Intell. Serv. Robot.*, vol. 13, pp. 1–14, 2020.

[14] A. Ghanbari, P. H. Chang, B. J. Nelson, and H. Choi, "Magnetic actuation of a cylindrical microrobot using time-delay-estimation closed-loop control: modeling and experiments.," *Smart Mater. Struct.*, vol. 23, no. 3, 2014.

[15] A. Ghanbari and M. Bahrami, "Nonlinear Modeling Application to Micro-/Nanorobotics," in *Nonlinear Approaches in Engineering Applications*, 2019, pp. 113–140.

[16] K. T. Nguyen, G. Go, E. Choi, B. Kang, J.-O. Park, and C.-S. Kim, "A Guide-Wired Helical Microrobot for Mechanical Thrombectomy: A Feasibility Study," in *2018 40th Annual International Conference of the IEEE Engineering in Medicine and Biology Society (EMBC)*, 2018.

[17] T. Yamanaka and F. Arai, "Self-Propelled Swimming Microrobot Using Electroosmotic Propulsion and Biofuel Cell," *IEEE Robot. Autom. Lett.*, vol. 3, no. 3, pp. 1787–1792, 2018.

[18] A. Hosney, A. Klingner, S. Misra, and I. S. M. Khalil, "Propulsion and steering of helical magnetic microrobots using two synchronized rotating dipole fields in three-dimensional space," in *2015 IEEE/RSJ International Conference on Intelligent Robots and Systems (IROS)*, 2015.

[19] S. JEON *et al.*, "Magnetically actuated microrobots as a platform for stem cell transplantation," *Sci. Robot.*, vol. 4, no. 30, 2019.

[20] P. B. Nguyen, J.-O. Park, S. Park, and S. Y. Ko, "Medical micro-robot navigation using image processing - blood vessel extraction and X-ray calibration," in *2016 6th IEEE International Conference on Biomedical Robotics and Biomechatronics (BioRob)*, 2016.

[21] J. A. Piepmeier, S. Firebaugh, and C. S. Olsen, "Uncalibrated Visual Servo Control of Magnetically Actuated Microrobots in a Fluid Environment," *Micromachines*, vol. 5, no. 4, pp. 797–813, 2014.

[22] M. E. Tiryaki, Ö. Erin, and M. Sitti, "A Realistic Simulation Environment for MRI-Based Robust Control of Untethered Magnetic Robots With Intra-Operational Imaging," *IEEE Robot. Autom. Lett.*, vol. 5, no. 3, pp. 4501–4508, 2020.

[23] M. B. Khamesee, N. Kato, Y. Nomura, and T. Nakamura, "Design and control of a microrobotic system using magnetic levitation," *IEEE/ASME Trans. Mechatronics*, vol. 7, no. 1, pp. 1–14, 2002.

[24] L. Arcese, M. Fruchard, and A. Ferreira, "Adaptive Controller and Observer for a Magnetic Microrobot," *IEEE Trans. Robot.*, vol. 29, no. 4, pp. 1060–1067, 2013.

[25] Z. Zhang, F. Long, and C. Menq, "Three-Dimensional Visual Servo Control of a Magnetically Propelled Microscopic Bead," *IEEE Trans. Robot.*, vol. 29, no. 2, pp. 373–382, 2013.

[26] L. Mellal, D. Folio, K. Belharet, and A. Ferreira, "Optimal control of multiple magnetic microbeads navigating in microfluidic channels," in *2016 IEEE International Conference on Robotics and Automation (ICRA)*, 2016.

[27] H. Marino, C. Bergeles, and B. J. Nelson, "Robust Electromagnetic Control of Microrobots Under Force and Localization Uncertainties," *IEEE Trans. Autom. Sci. Eng.*, vol. 11, no. 1, pp. 310–316, 2014.

[28] J. Kim, H. Choi, and J. Kim, "A Robust Motion Control With Antiwindup Scheme for Electromagnetic Actuated Microrobot Using Time-Delay Estimation," *IEEE/ASME Trans. Mechatronics*, vol. 24, no. 3, pp. 1096–1105, 2019.

[29] A. Ghanbari, P. H. Chang, B. J. Nelson, and H. Choi, "Electromagnetic Steering of a Magnetic Cylindrical Microrobot Using Optical Feedback Closed-Loop Control," *Int. J. Optomechatronics*, vol. 8, no. 2, pp. 129–145, 2014.

[30] B. Kosko, "Fuzzy Systems as Universal Approximators," *IEEE Trans. Comput.*, vol. 43, no. 11, pp. 1329–1333, 1994.

[31] K. J. Åström and B. Wittenmark, *Adaptive Control*. Addison-Wesley, 2008.

[32] A. Levant, "Robust Exact Differentiation via Sliding Mode Technique," *Automatica*, vol. 34, no. 3, pp. 379–384, 1998.